https://doi.org/10.1038/s42255-023-00866-z

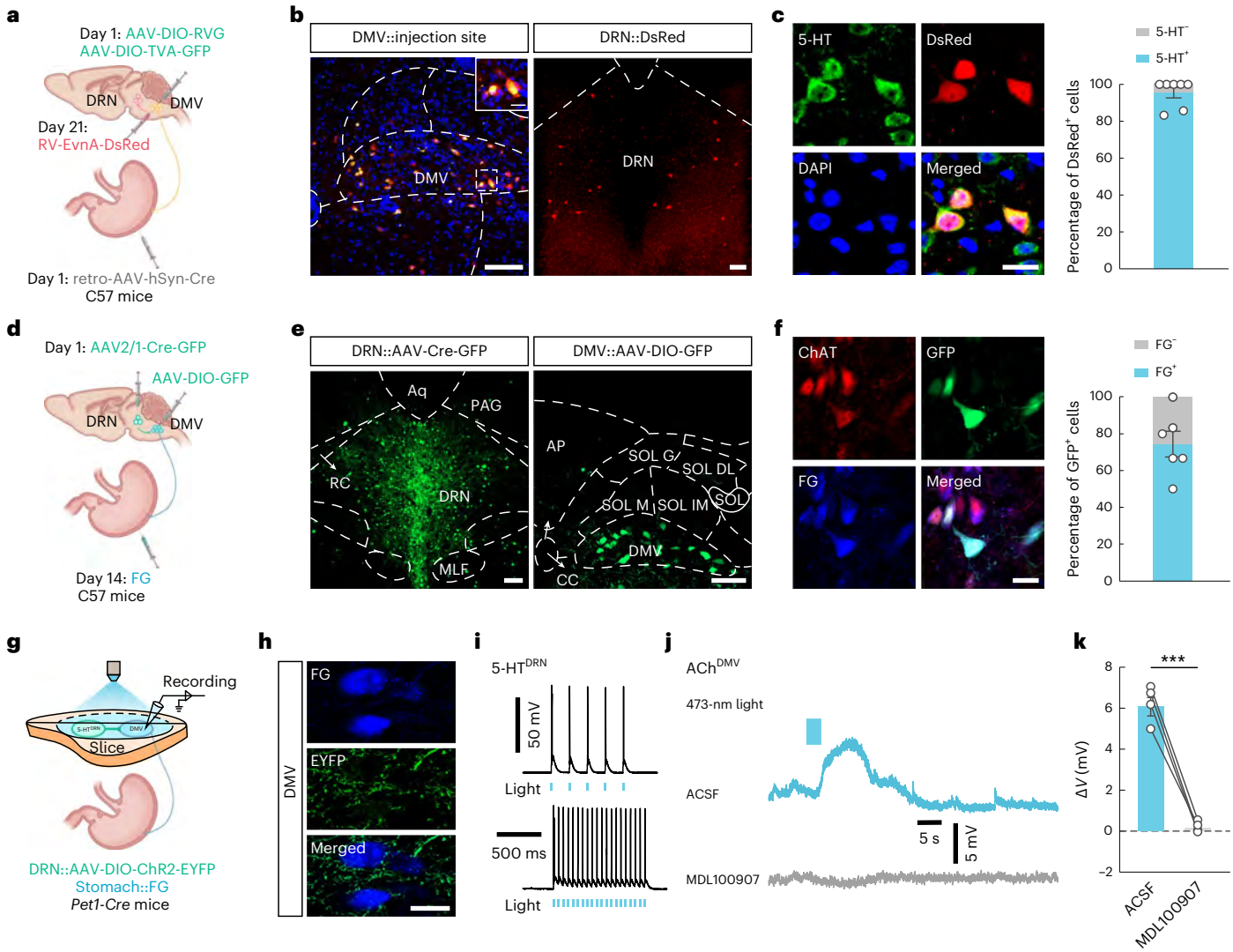

Fig. 3 | Defining the 5-HT^{DRN} → ACh^{DMV} → stomach circuits. a, Schematic of virus injection. **b**, Representative images of viral expression in the DMV (left) and DsRed-labelled neurons in the DRN (right). Scale bars, 100 μm. The inset depicts the area shown in the white box. Scale bar, 20 μm. **c**, Representative images and quantification analysis showing the DsRed-labelled neurons in the DRN traced from the DMV colocalized with 5-HT antibody ($n = 7$ brain slices). Scale bar, 20 μm. **d**, Schematic of virus injection. **e**, Typical images showing viral expression in the DRN and DMV. Scale bars, 100 μm. **f**, Typical images and quantification analysis showing the GFP-labelled neurons in the DMV traced from the DRN colocalized with FG signals and ChAT antibody ($n = 6$ brain slices). Scale bar, 20 μm. **g**, Schematic of viral injection and recording configuration in acute slices. **h**, Typical images showing EYFP$^+$ fibres in the DMV surrounding the FG signals. Scale bar, 20 μm. **i**, Sample traces of light-evoked action potentials recorded from EYFP$^+$ neurons in DRN acute brain slices. **j**,**k**, Representative traces (**j**) and summarized data (**k**) of light-evoked currents before and after treatment with MDL100907 (10 μM, $n = 5$ cells, $P < 0.0001$). In **k**, significance was assessed by two-tailed paired Student's *t*-tests. All data are presented as the mean ± s.e.m. ***$P < 0.001$. 12N, hypoglossal nucleus; ACSF, artificial cerebrospinal fluid; Aq, aqueduct; DL, dorsolateral part; G, gelatinous part; IM, intermediate part; M medial part; MLF, medial longitudinal fasciculus; PAG, periaqueductal grey; RC, raphe cap.

that the Ca^{2+} transient frequency of ACh^{DMV} neurons was significantly decreased after CS treatment in *ChAT-Cre* mice with infusion of AAV-DIO-GCaMP6m into the DMV (Extended Data Fig. 3e–g and Supplementary Video 2).

To record the DMV neurons that specifically project to the stomach, we performed microendoscopic experiments in mice with retro-AAV-Cre infused into the stomach and with AAV-DIO-GCaMP6m infused into the DMV (Fig. 2g and Extended Data Fig. 3h,i). We found that the Ca^{2+} transient frequency of the stomach-projecting DMV neurons was significantly decreased after CS (Fig. 2h). Whole-cell recordings in brain slices to assess the neuronal activity of visualized FG$^+$ neurons of the DMV tracing from the stomach also showed a decrease in firing rate and an increase in the rheobase in mice under CS compared with control mice (Extended Data Fig. 3j–l).

Given the decrease in ACh^{DMV} neuronal activity in mice under CS, we selectively activated stomach-projecting ACh^{DMV} neurons through (1) stomach infusion of retro-AAV-hSyn-Cre virus and DMV infusion of AAV-DIO-hM3Dq-mCherry in C57 mice, and (2) intraperitoneal injection with clozapine *N*-oxide (CNO) for seven successive days (Fig. 2i and Extended Data Fig. 4a–d). CS-induced gastric dysfunction was significantly reversed after activation of ACh^{DMV} neurons (Fig. 2j–l and Extended Data Fig. 4e–g). We also infused AAV-DIO-ChR2-EYFP in the DMV and implanted flexible wireless optoelectronic implants in the stomach of *ChAT-Cre* mice (Fig. 2m–o). Light stimulation of the ChR2-containing fibres around the gastric wall reliably induced a significant increase in the amplitude of gastric mobility (Fig. 2p,q). Collectively, these results revealed that a reduction in ACh^{DMV} neuronal activity contributed to CS-induced gastric dysfunction.